AIMS Mathematics

http://www.aimspress.com/journal/Math

AIMS Mathematics, 6(4): 3974–3995.
DOI: 10.3934/math.2021236
Received: 13 October 2020
Accepted: 26 January 2021
Published: 03 February 2021

Research article

Entropy solutions for an adaptive fourth-order nonlinear degenerate problem for noise removal

Abdelgader Siddig[1,2,*], **Zhichang Guo**[1], **Zhenyu Zhou**[1] **and Boying Wu**[1]

[1] Department of Mathematics, Harbin Institute of Technology, Harbin, 150001, China

[2] Department of Mathematics, University of Albutana, Ruffa'a, 420, Sudan

* **Correspondence:** Email: abdo2t@yahoo.com; Tel: +249117228600.

Abstract: Noise is regarded as an unavoidable component of digital image acquisition. Hence, noise removal has been considered as one of the fundamental tasks in the field of image processing. Accordingly, excellent results have been achieved by using second-order models. However, these outcomes are affected by the staircase effect. To eliminate this anomaly and maintaining the balance of removing noise and preserving edges, a fourth-order model is proposed. The existence and uniqueness of the entropy solution for this model are established. Besides, to to verify the effectiveness of the model in noise removal, we carried out numerical experiment and presented our results. Indeed, the experimental results show that our model is superior to PM model and ROF model in terms of removing noise and preserving edges.

Keywords: entropy solution; fourth-order PDE; noise removal; adaptive BV^2 space
Mathematics Subject Classification: 94A08, 65J15

1. Introduction

Noise is the most difficult task in the field of image processing and computer vision. In this work, we focus on removing additive Gaussian noise. The problem is formulated mathematically as: let $u(x, y)$ be a digital image and $u_0(x, y)$ be its observation with random noise $\eta(x, y)$. For $(x, y) \in \Omega$ s.t.

$$u_0(x, y) = u(x, y) + \eta(x, y). \tag{1.1}$$

The noise level is approximately known

$$\|u - u_0\|^2_{L^2(\Omega)} = \int_\Omega (u - u_0)^2 dx \approx \sigma^2. \tag{1.2}$$

The goal of denoising is to filter out high frequency signals, while preserving the important features of the image such as edges. Therefore, we search for an image processing model which removes noise and offers better handling of edges.

During the last two decades, the method of partial differential equations (PDEs) for image processing has become a major research topic. A classical PDEs model named ROF (Rudin, Osher, Fatemi) model which was based on the total variation (TV), was first introduced by Rudin et al. [18]. The idea in the ROF model is to minimize the the total variation of the image u,

$$\mathrm{TV} = \min_{u\in BV(\Omega)\cap L^2(\Omega)} \int_\Omega |\nabla u| dx + \frac{\lambda}{2}\int_\Omega (u-u_0)^2 dx. \tag{1.3}$$

In fact, one of the main advantages of using ROF model for image restoration is that the discontinuities are allowed. However, the main drawback of denoising models based on the TV is that they tend to yield piecewise constant images, a phenomenon known as staircase effects. Strong [19], introduced an adaptive TV functional (TV_α)

$$\mathrm{TV}_\alpha = \min_{u\in BV(\Omega)\cap L^2(\Omega)} \int_\Omega \alpha(x)|\nabla u(x)| dx + \frac{\lambda}{2}\int_\Omega (u-u_0)^2 dx, \tag{1.4}$$

for spatially adaptive image restoration. The function $\alpha(x)$ is an edge detector to control the diffusion. The main idea of edge detector is that edges of an image are associated with location of high gradient in a slightly smooth version of the noisy image.

In the recent decades, to overcome the staircase effects that caused by second-order variational model, fourth-order PDEs have been introduced in image restoration, [1–4, 9, 10, 12, 14, 16, 20, 22, 24–28]. You-Kaveh [26] proposed the following functional

$$\int_\Omega f(|\triangle u|) dxdy, \tag{1.5}$$

where $\triangle$ denote the Laplacian operator. Based on the gradient descent method, this second order functional yields a fourth-order PDE

$$u_t = -\triangle(g((\triangle u)^2)\triangle u), \tag{1.6}$$

where $g(s) = k^2/(k^2+s^2)$ and k is an image dependent parameter. This equation does avoid blocky piecewise constant solution. However, it produces speckles in the processed image [16]. Many other authors have considered image denoising models based on the minimizer of high-order functionals. Laysaker et al. [16] proposed the LLT model

$$\int_\Omega (|u_{xx}| + |u_{yy}|) dxdy, \tag{1.7}$$

and

$$\int_\Omega \sqrt{|u_{xx}|^2 + |u_{xy}|^2 + |u_{yx}|^2 + |u_{yy}|^2} dxdy, \tag{1.8}$$

they try to minimize the TV of ∇u. Minimizing these two functionals is equivalent to solve the following PDEs respectively

$$u_t = -\left(\frac{u_{xx}}{|\ u_{xx}\ |}\right)_{xx} - \left(\frac{u_{yy}}{|\ u_{yy}\ |}\right)_{yy} \tag{1.9}$$

and

$$u_t = -\left(\frac{u_{xx}}{|\ D^2u\ |}\right)_{xx} - \left(\frac{u_{xy}}{|\ D^2u\ |}\right)_{yx} - \left(\frac{u_{yx}}{|\ D^2u\ |}\right)_{xy} - \left(\frac{u_{yy}}{|\ D^2u\ |}\right)_{yy}, \tag{1.10}$$

where $|\ D^2u\ | = \sqrt{|u_{xx}|^2 + |u_{xy}|^2 + |u_{yx}|^2 + |u_{yy}|^2}$. These equations have proved to be the improved version of (1.6).

The theoretical analysis showed that fourth-order equations have advantages over second-order equations in some aspects. Fourth-order PDEs usually produce the smooth image of the observed image. This is believed to be a better approximation in smooth region. Therefore, the staircase effect is suggested to be reduced and the recovery image will look better. It is reasonable to conclude that fourth-order diffusion performs better than the second-order models in the aspect of the recovery of smooth regions.

In this paper, to address the problem of denoising images contaminated with additive noise, a fourth-order model is suggested. Using the gradient module of the image to design a speed controlling function. This function indicated where is the edge in the image, thus the new model can preserve edge in this region. The motivation for proposing this model is to overcome certain inconsistencies in second order models founded during the process of recovering smooth regions and better preservation of the fine details. The model is based on solving a nonlinear fourth order degenerate equation with the noisy image as its initial data. By use of Roth's method, we proved the existence and uniqueness of the entropy solution. Additionally, the numerical results demonstrate that the proposed model is superior to PM (Perona, Malik) [17] and ROF models.

The rest of this article is organized as follows. In Section 2, we give some preliminaries that we will use. Section 3 is devoted to the proposed model and the proofs of existence and uniqueness of its solution. The difference schemes are presented in Section 4. Numerical experiments are presented in Section 5 and the conclusion of this paper is given in Section 6.

2. Preliminaries

In this section, we recall some necessary definitions and notations, [11,13,14]. We begin with some definitions of the space BV^2, which consists of functions $u \in W^{1,1}(\Omega)$ s.t $\nabla u \in BV(\Omega)$, this space is also denoted by $BH(\Omega)$. To know more about space of bounded Hessian, we refer the reader to [4,5,8].

Definition 2.1. *Let $\Omega \subseteq \mathbb{R}^n$ be a bounded open domain with Lipschitz boundary. Let $u \in L^1(\Omega)$. Then the BV^2 semi-norm of u is characterized by*

$$\|D^2u\| = \sup_{\phi \in C_0^2(\Omega, \mathbb{R}^{n\times n})} \left\{ \int_\Omega \sum_{i,j=1}^{n} u\partial_j\partial_i\phi^{ij}dx : |\phi(x)| \le 1, \forall x \in \Omega \right\} < \infty, \tag{2.1}$$

where $C_0^2(\Omega, X)$ is the space of functions from Ω to X, 2-times continuously differentiable with compact support and $\phi(x)$is a vector valued function, with $|\phi(x)| = \sqrt{\sum_{i,j=1}^{n}(\phi^{ij})^2}$. Here we remark that the space BV^2 equipped with $\|u\|_{BV^2(\Omega)} = \|D^2u\| + \|u\|_{L^1(\Omega)}$ is a Banach space.

Definition 2.2. *Suppose that $\Omega \subseteq \mathbb{R}^n$ be a bounded open domain with Lipschitz boundary, $u \in L^1(\Omega)$,*

and $\alpha(x) \geq 0$ is continuous and real function. Then we define the weighted BV^2 semi-norm of u as

$$\|D^2u\|_\alpha = \sup_{\phi \in C_0^2(\Omega, \mathbb{R}^{n\times n})} \left\{ \int_\Omega \sum_{i,j=1}^{n} u\partial_j\partial_i\phi^{ij}dx : |\phi(x)| \leq \alpha, \forall x \in \Omega \right\} < \infty \tag{2.2}$$

3. The proposed model

In this section, we propose a fourth-order image denoising model, with some guidance from previous work [6, 14–16, 26, 27]. There are some benefits of fourth-order models. On the one hand, it can remove high frequency oscillation more effectively than second-order models because the evaluation of the second-order becomes weak in the high frequency area. One the other hand, for the fourth-order model, there is flexibility in employing different functional behaviors in the formulation.

Consider the following boundary value problem

$$\frac{\partial u}{\partial t} + D_{ij}^2\left(\frac{\alpha(x)\, D_{ij}^2 u}{|D_{ij}^2 u|}\right) = 0 \qquad (x,t) \in \Omega_T = (0,T)\times\Omega, \tag{3.1}$$

$$u(x,t) = 0, \qquad (x,t) \in (0,T)\times\partial\Omega, \tag{3.2}$$

$$\frac{\partial u}{\partial \overrightarrow{n}} = 0, \qquad (x,t) \in (0,T)\times\partial\Omega, \tag{3.3}$$

$$u(x,0) = u_0(x), \qquad x \in \Omega, \tag{3.4}$$

where $\alpha(x) = \frac{1}{\sqrt{1+|G_\sigma * \nabla u_0|^2}}$, $G_\sigma(x)$ is the Gaussian filter with parameter σ, $u_0(x)$ is the original image, Ω is bounded domain of $\mathbb{R}^2$ with appropriate smooth boundary, $T > 0$ is fixed, $\overrightarrow{n}$ denote the unit outward normal of the boundary $\partial\Omega$.

The term $\alpha(x)$ is used to enhance edges. In fact, it controls the speed of the diffusion: in the smooth region where ∇u_0 is small, the diffusion is strong. Near possible edges, however, where ∇u_0 is large, the diffusion spread is low. The convolution with G_σ should smooth away any large oscillations of noise. Therefore, we can get the smooth image and further preserve the edges in a best way.

Definition 3.1. *A measurable function $u : \Omega_T \to \mathbb{R}$ is an entropy solution of (3.1)–(3.4) in Ω_T if $u \in C([0,T]; L^2(\Omega)) \cap L^\infty(0,T; BV^2(\Omega))$, $\frac{\partial u}{\partial t} \in L^2(\Omega_T)$ and there exist z, such that $\alpha z \in L^\infty(\Omega_T)$ with $\| \alpha\, z \|_{L^\infty(\Omega_T)} \leq 1$, $u_t + D_{ij}\alpha z_{ij} = 0$ in $D'(\Omega_T)$ such that*

$$\int_\Omega (u(t) - v)u_t dx \leq \int_\Omega \alpha z(t)\cdot D^2 v dx - \|D^2u\|_\alpha, \tag{3.5}$$

for every $v \in L^\infty(0,T; W_0^{2,1}(\Omega))$.

Before investigating the existence and uniqueness of problem (3.1)–(3.4), let us consider the following approximate evaluation problem: for $1 < p \leq 2$ and $u_{0p} \in W^{2,p}(\Omega)$, we construct the following problem

$$\frac{\partial u_p}{\partial t} + D_{ij}^2\left(\alpha(x)|D_{ij}^2 u_p|^{p-2}D_{ij}^2 u_p\right) = 0, \qquad (x,t) \in \Omega_T \tag{3.6}$$

$$u_p(x,t) = 0, \qquad (x,t) \in (0,T)\times\partial\Omega, \tag{3.7}$$

$$\frac{\partial u_p}{\partial \overrightarrow{n}} = 0, \qquad (x,t) \in (0,T)\times\partial\Omega, \tag{3.8}$$

$$u_p(x,0) = u_{0p}(x), \qquad x \in \Omega. \tag{3.9}$$

Lemma 3.1. *For any fixed p, $1 < p \le 2$, the above problem* (3.6)–(3.9) *admits a weak solution $u_p \in L^\infty(0,T;W_0^{2,p}(\Omega)) \cap C([0,T];L^2(\Omega))$ and $\frac{\partial u_p}{\partial t} \in L^2(\Omega_T)$ such that*

$$\lim_{t\to 0^+} \| u_p(x,t) - u_{0p}(x) \|_{L^2(\Omega)} = 0, \tag{3.10}$$

and for any $\varphi \in C_0^\infty(\Omega_T)$ the following integral equality holds

$$\int_0^T \int_\Omega \frac{\partial u_p}{\partial t}\varphi(x,t)dxdt + \int_0^T \int_\Omega \alpha(x)|\, D_{ij}^2 u_p|^{p-2}\, D_{ij}^2 u_p \cdot D_{ij}^2\varphi(x,t)dxdt = 0, \tag{3.11}$$

with

$$\| u_p \|_{L^\infty(0,T;W_0^{2,p}(\Omega))} + \| u_p \|_{L^\infty(0,T;L^2(\Omega))} + \left\| \frac{\partial u_p}{\partial t} \right\|_{L^2(\Omega_T)} \le C, \tag{3.12}$$

where C is a constant independent of p.

Proof. We apply Rothe's method [23], to construct an approximate solution sequence. Divide the interval $[0,T]$ into n equal segments and define $h = \frac{T}{n}$. For any j: $1 \le j \le n$, for any positive integer n and a function $u(x,t)$, denote

$$u_p^{n,j}(x) = u_p(x, jh), \qquad j = 1, 2, ..., n.$$

For fixed j, define the following functional on $W_0^{2,p}(\Omega)$

$$E(w) = \frac{1}{p}\int_\Omega \alpha(x)|D_{ij}^2 w|^p dx + \frac{1}{2h}\int_\Omega (w - u_p^{n,j-1})^2 dx. \tag{3.13}$$

The idea here is to prove that if $u_p^{n,j-1}$ is known and $u_p^{n,0} = u_{0p}$, then there is a minimizer for (3.13). Let $u_m \in W_0^{2,p}(\Omega)\cap L^2(\Omega)$ be a minimizing sequence for E. Since α is bounded below, then the sequence u_m is bounded in $W_0^{2,p}(\Omega)$ and $L^2(\Omega)$. Therefore, there exists a subsequence $u_{m_i}$of u_m and a function $u_p^{n,j} \in W_0^{2,p}(\Omega) \cap L^2(\Omega)$ such that as $i \to \infty$,

$$u_{m_i} \to u_p^{n,j} \text{ weakly in } W_0^{2,p}(\Omega) \text{ and } L^2(\Omega). \tag{3.14}$$

From this and the weak lower semicontinuity of the norms, we get

$$E(u_p^{n,j}) \le \liminf_{i\to\infty} E(u_{m_i}) = \inf_{w\in W_0^{2,p}(\Omega)\cap L^2(\Omega)} E(w).$$

Then $u_p^{n,j}$ is the solution of the Euler equation corresponding to $E(w)$

$$D_{ij}^2\left(\alpha(x)|D_{ij}^2u_p^{n.j}|^{p-2}D_{ij}^2u_p^{n.j}\right)+\frac{1}{h}(u_p^{n.j}-u_p^{n,j-1})=0, \tag{3.15}$$

which implies

$$\frac{1}{h}\int_\Omega(u_p^{n,j}-u_p^{n,j-1})\eta(x)dx+\int_\Omega\alpha(x)|D_{ij}^2u_p^{n,j}|^{p-2}\ D_{ij}^2u_p^{n,j}\cdot D_{ij}^2\eta(x)dx=0, \tag{3.16}$$

for any $\eta(x)\in C_0^\infty(\Omega)$.

Let $\chi^{n,j}(t)$ be the indicator function of $[h(j-1),hj)$ and

$$\lambda^{n,j}(t)=\begin{cases}\frac{t}{h}-(j-1), & \text{if } t\in[h(j-1),hj),\\ 0, & \text{otherwise.}\end{cases}$$

We construct an approximation function as

$$u_p^n(x,t)=\sum_{j=1}^n\chi^{n,j}(t)u_p^{n,j},\ \text{with}\qquad u_p^n(x,0)=u_{0p}(x)$$

and

$$w_p^n(x,t)=\sum_{j=1}^n\chi^{n,j}(t)[u_p^{n,j-1}(x)+\lambda^{n,j}(t)(u_p^{n,j}(x)-u_p^{n,j-1}(x))].$$

By (3.16), we have

$$\int_\Omega\left(\frac{\partial w_p^n}{\partial t}\eta(x)+\alpha(x)|D_{ij}^2u_p^n\ |^{p-2}\ D_{ij}^2u_p^n\cdot D_{ij}^2\eta(x)\right)dx=0,$$

for every $\eta(x)\in C_0^\infty(\Omega)$ a.e. $t\in[0,T]$, which implies that

$$\int_0^T\int_\Omega\left(\frac{\partial w_p^n}{\partial t}\varphi(x,t)+\alpha(x)|D_{ij}^2u_p^n|^{p-2}D_{ij}^2u_p^n\cdot D_{ij}^2\varphi(x,t)\right)dxdt=0, \tag{3.17}$$

for every $\varphi\in C_0^\infty(\Omega_T)$.

Next, we obtain some estimates for $u_p^n(x,t)$ and $w_p^n(x,t)$. Notice that, we choose $\eta(x)\in W_0^{2,p}(\Omega)$ as the test function in (3.16). Let $\eta(x)=u_p^{n,j}-u_p^{n,j-1}$, we have

$$\frac{1}{h}\int_\Omega(u_p^{n,j}-u_p^{n,j-1})^2dx+\int_\Omega\alpha(x)|D_{ij}^2u_p^{n,j}|^{p-2}\ D_{ij}^2u_p^{n,j}\cdot D_{ij}^2(u_p^{n,j}-u_p^{n,j-1})dx=0,$$

$$\frac{1}{h}\int_\Omega(u_p^{n,j}-u_p^{n,j-1})^2dx+\int_\Omega\alpha(x)|D_{ij}^2u_p^{n,j}|^pdx=\int_\Omega\alpha(x)|D_{ij}^2u_p^{n,j}|^{p-2}\ D_{ij}^2u_p^{n,j}\cdot D_{ij}^2u_p^{n,j-1}dx.$$

Using Young's inequality, we have

$$\frac{1}{h}\int_\Omega(u_p^{n,j}-u_p^{n,j-1})^2dx+\int_\Omega\alpha(x)|D_{ij}^2u_p^{n,j}|^pdx\le\frac{p-1}{p}\int_\Omega\alpha(x)|D_{ij}^2u_p^{n,j}|^pdx+\frac{1}{p}\int_\Omega\alpha(x)|D_{ij}^2u_p^{n,j-1}|^pdx.$$

That is

$$\frac{1}{h}\int_\Omega (u_p^{n,j}-u_p^{n,j-1})^2dx+\frac{1}{p}\int_\Omega \alpha(x)|D_{ij}^2u_p^{n,j}|^pdx\le\frac{1}{p}\int_\Omega \alpha(x)|D_{ij}^2u_p^{n,j-1}|^pdx. \tag{3.18}$$

For any m with $1\le m\le n$, summing (3.18) for j from 1 to m

$$\int_\Omega \alpha(x)|D_{ij}^2u_p^{n,m}|^pdx\le\int_\Omega \alpha(x)|D_{ij}^2u_{0p}|^pdx,$$

which implies

$$\sup_{0<t<T}\|D_{ij}^2u_p^n\|^p_{W_0^{2,p}(\Omega)}\le C, \tag{3.19}$$

where C is a constant independent of p,n.
Summing (3.18) for j from 1 to n yield

$$\frac{1}{h}\sum_{j=1}^n\int_\Omega (u_p^{n,j}-u_p^{n,j-1})^2dx\le\frac{1}{p}\int_\Omega \alpha(x)|D_{ij}^2u_{0p}|^pdx=C. \tag{3.20}$$

By the definition of $w_p^n(x,t)$, we have

$$\frac{\partial w_p^n}{\partial t}=\frac{1}{h}\sum_{j=1}^n\chi^{n,j}(t)(u_p^{n,j}-u_p^{n,j-1}).$$

Thus

$$\left\|\frac{\partial w_p^n}{\partial t}\right\|^2_{L^2(\Omega_T)}=\frac{1}{h^2}\sum_{j=1}^n h\|(u_p^{n,j}-u_p^{n,j-1})\|^2_{L^2(\Omega)}\le C. \tag{3.21}$$

By (3.19), we can obtain

$$\begin{aligned}\sup_{0<t<T}\int_\Omega|\,D_{ij}^2w_p^n|^pdx&=\sup_{0<t<T}\sum_{j=1}^n\chi^{n,j}(t)\int_\Omega|(1-\lambda^{n,j}(t))\,D_{ij}^2u_p^{n,j-1}+\lambda^{n,j}(t)\,D_{ij}^2u_p^{n,j}|^pdx\\&\le\sup_{0<t<T}\|\,D_{ij}^2u_p^n\|^p_{W_0^{2,p}(\Omega)}\le C.\end{aligned} \tag{3.22}$$

Choosing $\eta(x)=u_p^{n,j}$ in (3.16), we get

$$\frac{1}{h}\int_\Omega (u_p^{n,j}-u_p^{n,j-1})u_p^{n,j}dx+\int_\Omega\alpha(x)|D_{ij}^2u_p^{n,j}|^{p-2}\,D_{ij}^2u_p^{n,j}\cdot D_{ij}^2u_p^{n,j}dx=0,$$

which implies

$$\frac{1}{h}\int_\Omega (u_p^{n,j}-u_p^{n,j-1})u_p^{n,j}dx+\int_\Omega\alpha(x)|D_{ij}^2u_p^{n,j}|^pdx=0.$$

By Young's inequality, we have

$$h\int_\Omega\alpha(x)|D_{ij}^2u_p^{n,j}|^pdx+\frac{1}{2}\int_\Omega|u_p^{n,j}|^2dx\le\frac{1}{2}\int_\Omega|u_p^{n,j-1}|^2dx. \tag{3.23}$$

Thus

$$\int_\Omega|u_p^{n,j}|^2dx\le\int_\Omega|u_p^{n,j-1}|^2dx. \tag{3.24}$$

This implies

$$\sup_{0<t<T}\int_\Omega |u_p^n|^2 dx \le \int_\Omega |u_{0p}|^2 dx. \tag{3.25}$$

Similar to the proof of (3.22), we also see

$$\sup_{0<t<T}\int_\Omega |w_p^n|^2 dx \le \int_\Omega |u_{0p}|^2 dx. \tag{3.26}$$

Choosing $\eta(x) = u_p^{n,j-1}$ in (3.16)

$$\int_\Omega (u_p^{n,j} - u_p^{n,j-1})u_p^{n,j-1}dx + h\int_\Omega \alpha(x)|D_{ij}^2 u_p^{n,j}|^{p-2}\, D_{ij}^2 u_p^{n,j}\cdot D_{ij}^2 u_p^{n,j-1}dx = 0.$$

Applying Hölder's inequality and the estimate (3.19), we have

$$\int_\Omega (u_p^{n,j-1} - u_p^{n,j})u_p^{n,j-1}dx \le Ch.$$

By Young's inequality again yields

$$\int_\Omega |u_p^{n,j-1}|^2 dx \le Ch + \frac{1}{2}\int_\Omega |u_p^{n,j-1}|^2 dx + \frac{1}{2}\int_\Omega |u_p^{n,j}|^2 dx.$$

Thus

$$-Ch \le \int_\Omega |u_p^{n,j}|^2 dx - \int_\Omega |u_p^{n,j-1}|^2 dx. \tag{3.27}$$

Define $B(u_p^n) = \alpha(x)|\, D_{ij}^2 u_p^n|^{p-2}\, D_{ij}^2 u_p^n$. Combining (3.19), (3.21), (3.22), (3.25) and (3.26), we conclude that there exist subsequences of $u_p^n, w_p^n, \frac{\partial w_p^n}{\partial t}$ and $B(u_p^n)$, denoted by themselves such that, as $n \to \infty$

$$\begin{aligned}
&u_p^n \overset{*}{\rightharpoonup} u_p, \quad \text{in} \quad L^\infty(0,T;W_0^{2,p}(\Omega)),\\
&w_p^n \overset{*}{\rightharpoonup} w_p, \quad \text{in} \quad L^\infty(0,T;W_0^{2,p}(\Omega)),\\
&\frac{\partial w_p^n}{\partial t} \rightharpoonup \frac{\partial w_p}{\partial t}, \quad \text{in} \quad L^2(\Omega_T),\\
&B(u_p^n) \overset{*}{\rightharpoonup} \zeta, \quad \text{in} \quad L^\infty(0,T;L^{p'}(\Omega)),
\end{aligned} \tag{3.28}$$

holds for some u_p, w_p, ζ. And we also have

$$\|w_p\|^p_{L^\infty(0,T;W_0^{2,p}(\Omega))} + \left\|\frac{\partial w_p}{\partial t}\right\|^2_{L^2(\Omega_T)} + \|u_p\|^p_{L^\infty(0,T;W_0^{2,p}(\Omega))} \le C. \tag{3.29}$$

Then let $n \to \infty$ in (3.17),

$$\frac{\partial w_p}{\partial t} + D_{ij}^2\zeta = 0. \tag{3.30}$$

Next, we show that $u_p = w_p$. By the definition of u_p and w_p, we have

$$w_p^n - u_p^n = \sum_{j=1}^{n} \chi^{n,j}(t)(1 - \lambda^{n,j}(t))(u_p^{n,j-1} - u_p^{n,j}),$$

which combined with (3.20), leads to

$$\|w_p^n - u_p^n\|^2_{L^2(\Omega_T)} \leq \sum_{j=1}^{n} h\|u_p^{n,j} - u_p^{n,j-1}\|^2_{L^2(\Omega_T)} \leq Ch^2 \to 0, \text{ as } h \to 0. \tag{3.31}$$

Now, it remains to show that $\zeta = B(u_p)$. From (3.17) and the convergence sets (3.28), as $n \to \infty$, we can get

$$\int_0^T \int_\Omega \frac{\partial u_p}{\partial t}\varphi(x,t)dxdt + \int_0^T \int_\Omega \zeta.D_{ij}^2\varphi(x,t)dxdt = 0. \tag{3.32}$$

For any $g \in L^p(0,T,W^{2,p}(\Omega))$ and for j from 1 to n, we can obtain, by the monotonicity condition, the inequality

$$\int_\Omega (B(u_p^{n.j}) - B(g))(D_{ij}^2 u_p^{n.j} - D_{ij}^2 g)dx \geq 0. \tag{3.33}$$

Letting $\eta = u_p^{n.j}$ in (3.16), we obtain

$$\frac{1}{h}\int_\Omega (u_p^{n,j} - u_p^{n,j-1})u_p^{n,j}dx + \int_\Omega B(u_p^{n,j}) \cdot D_{ij}^2 u_p^{n,j}dx = 0. \tag{3.34}$$

Applying Young's inequality on the first term of (3.34) together with the inequality (3.33) and integrating over $((j-1)h, jh)$, we get

$$\frac{1}{2}\int_\Omega \left[|u_p^{n,j}|^2 - |u_p^{n,j-1}|^2\right]dx + \int_{(j-1)h}^{jh}\int_\Omega B(u_p^{n,j})\cdot D_{ij}^2 g dxdt + \int_{(j-1)h}^{jh}\int_\Omega B(g)(D_{ij}^2 u_p^{n.j} - D_{ij}^2 g)dxdt \leq 0. \tag{3.35}$$

Summing up (3.35) for j from 1 to n, we obtain

$$\frac{1}{2}\int_\Omega \left[|u_p^n(T)|^2 - |u_{0p}|^2\right]dx + \int_0^T \int_\Omega B(u_p^n) \cdot D_{ij}^2 g dxdt + \int_0^T \int_\Omega B(g)(D_{ij}^2 u_p^n - D_{ij}^2 g)dxdt \leq 0. \tag{3.36}$$

Recalling the convergence sets (3.28) and letting $n \to \infty$, (3.36) yields

$$\frac{1}{2}\int_\Omega \left[|u_p(T)|^2 - |u_{0p}|^2\right]dx + \int_0^T \int_\Omega \zeta \cdot D_{ij}^2 g dxdt + \int_0^T \int_\Omega B(g)(D_{ij}^2 u_p - D_{ij}^2 g)dxdt \leq 0. \tag{3.37}$$

We can rewrite (3.37) in the form

$$\int_0^T \int_\Omega \frac{\partial u_p}{\partial t}u_p dxdt + \int_0^T \int_\Omega \zeta \cdot D_{ij}^2 g dxdt + \int_0^T \int_\Omega B(g)(D_{ij}^2 u_p - D_{ij}^2 g)dxdt \leq 0. \tag{3.38}$$

Letting $\varphi = u_p$ in (3.32), we obtain

$$\int_0^T \int_\Omega \frac{\partial u_p}{\partial t}u_p dxdt + \int_0^T \int_\Omega \zeta \cdot D_{ij}^2 u_p dxdt = 0. \tag{3.39}$$

Then, substituting (3.39) into (3.38) leads to

$$\int_0^T \int_\Omega (\zeta - B(g))(D_{ij}^2 u_p - D_{ij}^2 g)dxdt \geq 0. \tag{3.40}$$

Choose $g = u_p - ks$ where $k > 0$ and $D_{ij}^2 s \in L^\infty(0, T; W^{2,p}(\Omega))$. We then have

$$\int_0^T \int_\Omega (\zeta - B(u_p - ks))D_{ij}^2 s dxdt \geq 0. \tag{3.41}$$

Sending $k \to 0$, we obtain

$$\int_0^T \int_\Omega (\zeta - B(u_p))D_{ij}^2 s dxdt \geq 0, \ \forall s \in L^\infty(0, T; W^{2,p}(\Omega)). \tag{3.42}$$

Since s is arbitrary, we see that $\zeta = B(u_p)$.

Now, we prove (3.10), we let $\varphi = u_p(x, t)$ and $\varphi = u_p(x, t_1)$ in (3.32), for $0 \leq t_1 \leq t \leq t_2 \leq T$, we obtain

$$\int_\Omega \left(u_p^2(x, t_2) - u_p^2(x, t_1)\right) dx = -2 \int_{t_1}^{t_2} \int_\Omega \alpha(x) |\ D_{ij}^2 u_p|^p dxdt,$$

and

$$\int_\Omega u_p(x, t_2)u_p(x, t_1)dx - \int_\Omega u_p^2(x, t_1)dx = - \int_{t_1}^{t_2} \int_\Omega \alpha(x) |\ D_{ij}^2 u_p|^{p-2}\ D_{ij}^2 u_p . D_{ij}^2 u_p(x, t_1)dxdt.$$

Then

$$\begin{aligned}\int_\Omega |u_p(x, t_2) - u_p(x, t_1)|^2 dx &= \int_\Omega \left(u_p^2(x, t_2) - u_p^2(x, t_1)\right) dx + 2 \int_\Omega \left(u_p^2(x, t_1) - u_p(x, t_2)u_p(x, t_1)\right) dx, \\ &= -2 \int_{t_1}^{t_2} \int_\Omega \alpha(x) |\ D_{ij}^2 u_p|^p dxdt + 2 \int_{t_1}^{t_2} \int_\Omega \alpha(x) |\ D_{ij}^2 u_p|^{p-2}\ D_{ij}^2 u_p . D_{ij}^2 u_p(x, t_1)dxdt.\end{aligned}$$

From the above equation, we deduce that

$$\lim_{t \to 0^+} \| u_p(x, t) - u_{0p}(x) \|_{L^2(\Omega)} = 0,$$

and the proof is completed. □

Theorem 3.1. *If $u_0 \in BV^2(\Omega)$ and $u_0 = 0, \frac{\partial u}{\partial n} = 0, x \in \partial\Omega$ in the sense of trace then the problem* (3.1)–(3.4) *admits one and only one entropy solution.*

Proof. By Lemma 3.1, there exists u_p, which is a weak solution of the problem (3.6)–(3.9) and a constant C such that

$$\| u_p \|_{L^\infty(0,T;W_0^{2,p}(\Omega))} + \| u_p \|_{L^\infty(0,T;L^2(\Omega))} + \left\| \frac{\partial u_p}{\partial t} \right\|_{L^2(\Omega_T)} \leq C. \tag{3.43}$$

So, from (3.43), there exists a subsequence of u_p, denoted by itself and a function $u \in L^\infty(0, T; BV^2(\Omega)) \cap C([0, T]; L^2(\Omega))$ with $\frac{\partial u}{\partial t} \in L^2(\Omega_T)$ such that, as $p \to 1^+$,

$$u_p \to u, \text{in } W^{1,1}(\Omega), \text{ with } \|D^2u\|_\alpha \le \liminf_{p\to 1^+} \|D^2_{ij}u_p\|_{L^p(\Omega)}, \text{ a.e. } t \in (0,T)$$

and

$\frac{\partial u_p}{\partial t} \rightharpoonup \frac{\partial u}{\partial t}$, weakly in $L^2(\Omega_T)$.

We also have $u_p \to u$ strongly in $L^2(\Omega_T)$ a.e. $t \in (0,T)$ and

$$\lim_{t\to 0^+} \|u(x,t) - u_0(x)\|_{L^2(\Omega)} = 0.$$

Applying the method in [7], we next prove that $\alpha(x)|D^2_{ij}u_p|^{p-2}\, D^2_{ij}u_p$ is weakly relatively compact in $L^1(\Omega_T)$. Employing (3.43) and Hölder's inequality,

$$\left|\int_0^T \int_\Omega \alpha(x)|D^2_{ij}u_p|^{p-2}D^2_{ij}u_p dxdt\right| \le \int_0^T \int_\Omega |\ \alpha(x)\ ||\ D^2_{ij}u_p\ |^{p-1}\ dxdt \le C^{\frac{p-1}{p}} \text{meas}(\Omega_T)^{\frac{1}{p}},$$

where C is independent of p. Thus, $\left\{\alpha(x)|D^2_{ij}u_p|^{p-2}D^2_{ij}u_p\right\}$ is bounded and equi-integrable in $L^1(\Omega_T)$ and is therefore weakly relatively compact in $L^1(\Omega_T)$. Thus we deduce that as $p \to 1^+$,

$\left\{\alpha(x)|D^2_{ij}u_p|^{p-2}\, D^2_{ij}u_p\right\} \rightharpoonup \alpha z$, weakly in $L^1(\Omega_T)$.

So we get by Lemma 3.1 and the fact that $\frac{\partial u_p}{\partial t} \rightharpoonup \frac{\partial u}{\partial t}$ in $L^2(\Omega_T)$,

$$\int_0^T \int_\Omega \frac{\partial u}{\partial t}\varphi(x,t)dxdt + \int_0^T \int_\Omega \alpha z \cdot D^2_{ij}\varphi(x,t)dxdt = 0, \tag{3.44}$$

for every $\varphi(x,t) \in C_0^\infty(\Omega_T)$ and $u_t + D_{ij}\alpha z_{ij} = 0$ in $D'(\Omega_T)$.

Now, it remains to prove that $\|\ \alpha z\ \|_{L^\infty(\Omega_T)} \le 1$.

For any $k > 0$, setting

$A_{p,k} = \{(x,t) \in \Omega_T :|\ D^2_{ij}u_p\ |> k\}$, we have that

$$\text{meas}(A_{p,k}) \le \frac{C}{k^p}, \text{ for every } p > 1, k > 0.$$

As above, there exists a function $g_k \in L^1(\Omega_T)$ such that

$\alpha(x)|D^2_{ij}u_p|^{p-2}\, D^2_{ij}u_p\chi_{A_{p,k}} \rightharpoonup g_k$, as $p \to 1^+$ weakly in $L^1(\Omega_T)$,

where $\chi_{A_{p,k}}$ is the indicator function of $A_{p,k}$. Now for any $\phi \in L^\infty(\Omega_T)$ with $\|\phi\|_{L^\infty(\Omega_T)} \le 1$, by the definition of $\chi_{A_{p,k}}$, we see that

$$\left|\int_0^T \int_\Omega \alpha(x)|D^2_{ij}u_p|^{p-2}\, D^2_{ij}u_p\phi\chi_{A_{p,k}}dxdt\right| \le \frac{C}{k}.$$

Letting $p \to 1^+$, we have

$$\int_0^T \int_\Omega |\ g_k\ |\ dxdt \le \frac{C}{k}, \text{for every } k > 0. \tag{3.45}$$

Since we have that

$$\left|\int_0^T \int_\Omega \alpha(x)|D^2_{ij}u_p|^{p-2}\, D^2_{ij}u_p\chi_{\Omega_T/A_{p,k}}\right| \le k^{p-1}, \text{ for any } p > 1,$$

letting $p \to 1^+$, we obtain that $\alpha(x) \mid D^2_{ij}u_p \mid^{p-2} D^2_{ij}u_p\chi_{\Omega_T/A_{p,k}}$ weakly converges in $L^1(\Omega_T)$ to some function $f_k \in L^1(\Omega_T)$ with $\|f_k\|_{L^\infty(\Omega_T)} \le 1$. Since, for any $k > 0$, we may write $\alpha z = f_k + g_k$ with $\|f_k\|_{L^\infty(\Omega_T)} \le 1$ and g_k satisfies (3.45), it is easily follows that $\|\alpha z\|_{L^\infty(\Omega_T)} \le 1$.

Next, we verify the solution definition inequality (3.5). For any $v_n \in C_0^\infty(\Omega_T)$ and taking $\varphi = (u_p - v_n)\xi(t)$ in (3.11), we have

$$\int_0^T \int_\Omega \frac{\partial u_p}{\partial t}(u_p - v_n)\xi(t)dxdt = -\int_0^T \int_\Omega \alpha(x)|D^2_{ij}u_p|^{p-2} D^2_{ij}u_p \cdot D^2_{ij}((u_p - v_n)\xi(t))dxdt.$$

Letting $p \to 1^+$,

$$\int_0^T \int_\Omega \frac{\partial u}{\partial t}(u(t) - v_n)\xi(t)dxdt \le \int_0^T \int_\Omega \alpha z(t) \cdot D^2_{ij}v_n\xi(t)dxdt - \int_0^T \|D^2u\|_\alpha \xi(t)dt.$$

Then for any $v \in L^\infty(0,T; W_0^{2,1}(\Omega))$, letting $n \to \infty$,

$$\int_0^T \int_\Omega \frac{\partial u}{\partial t}(u(t) - v)\xi(t)dxdt \le \int_0^T \int_\Omega \alpha z(t) \cdot D^2_{ij}v\xi(t)dxdt - \int_0^T \|D^2u\|_\alpha \xi(t)dt.$$

Since $\xi(t)$ is arbitrary, we have

$$\int_\Omega \frac{\partial u}{\partial t}(u(t) - v)dx \le \int_\Omega \alpha z(t) \cdot D^2_{ij}vdx - \|D^2u\|_\alpha,$$

for every $v \in L^\infty(0,T; W_0^{2,1}(\Omega))$ and a.e. on $[0,T]$.

Finally, we prove the uniqueness of the entropy solution. Let u_1, u_2 both be entropy solution with data u_{10}, u_{20}. Then there exists $\alpha z_1, \alpha z_2 \in L^\infty(\Omega_T)$ such that

$$\int_\Omega \frac{\partial u_1}{\partial t}(u_1 - v)dx \le \int_\Omega \alpha z_1 \cdot D^2_{ij}vdx - \|D^2u_1\|_\alpha, \tag{3.46}$$

and

$$\int_\Omega \frac{\partial u_2}{\partial t}(u_2 - v)dx \le \int_\Omega \alpha z_2 \cdot D^2_{ij}vdx - \|D^2u_2\|_\alpha, \tag{3.47}$$

for every $v \in L^\infty(0,T; W_0^{2,1}(\Omega))$ and a.e. on $[0,T]$. Let $u_{1n}, u_{2n} \in L^\infty(0,T; W_0^{2,p}(\Omega))$ be approximates functions, respectively, for u_1 and u_2, such that

$$\lim_{n\to\infty}\left(\|D^2_{ij}u_{1n}\|_{L^1(\Omega)} - \|D^2u_1\|_\alpha\right) = 0, \lim_{n\to\infty} \| u_{1n} - u_1 \|_{L^2(\Omega)} = 0,$$

and

$$\lim_{n\to\infty}\left(\|D^2_{ij}u_{2n}\|_{L^1(\Omega)} - \|D^2u_2\|_\alpha\right) = 0, \lim_{n\to\infty} \| u_{2n} - u_2 \|_{L^2(\Omega)} = 0,$$

a.e. on$[0,T]$. Taking $v = u_{2n}$ in (3.46) and $v = u_{1n}$ in (3.47), adding the two equations and rearranging the result, we obtain

$$\begin{aligned}\int_\Omega (u_1 - u_2)\left(\frac{\partial u_1}{\partial t} - \frac{\partial u_2}{\partial t}\right)dx + \int_\Omega (u_1 - u_{1n})\frac{\partial u_2}{\partial t}dx + \int_\Omega (u_2 - u_{2n})\frac{\partial u_1}{\partial t}\\ \le \int_\Omega \alpha z_1 \cdot D^2_{ij}u_{2n}dx - \|D^2u_1\|_\alpha + \int_\Omega \alpha z_2 \cdot D^2_{ij}u_{1n}dx - \|D^2u_2\|_\alpha.\end{aligned}$$

So integrating from 0 to t and letting $n \to \infty$, we get

$$\int_\Omega (u_1 - u_2)^2 dx \le \int_\Omega (u_{10} - u_{20})^2 dx.$$

The proof is completed . □

4. Difference schemes

In this section, assuming τ to be the time step size and h the space grid size, we discretize time and space as follows:

$$\begin{aligned} t &= n\tau, \qquad n = 0, 1, 2, \cdots, \\ x &= ih, \qquad i = 0, 1, 2, \cdots, I, \\ y &= jh, \qquad j = 0, 1, 2, \cdots, J, \end{aligned}$$

where $Ih \times Jh$ is the size of the original image. Let $u^n_{i,j}$ denote approximations of $u(n\tau, ih, jh)$. We define the discrete approximation:

$$\begin{aligned} \triangle_x u^n_{i,j} &= \frac{u^n_{i+1,j} - 2u^n_{i,j} + u^n_{i-1,j}}{h^2}, \\ \triangle_y u^n_{i,j} &= \frac{u^n_{i,j+1} - 2u^n_{i,j} + u^n_{i,j-1}}{h^2}, \\ \triangle_{xy} u^n_{i,j} &= \frac{u^n_{i+1,j+1} + u^n_{i,j} - u^n_{i,j+1} - u^n_{i+1,j}}{h^2}. \end{aligned}$$

The discrete explicit scheme of the problem can be written as

$$\begin{aligned} u^{n+1}_{i,j} &= u^n_{i,j} - \tau \left[\triangle_x \left(\alpha_{ij} \frac{\triangle_x u^n_{i,j}}{|\triangle_x u^n_{i,j}|_\epsilon} \right) + \triangle_y \left(\alpha_{ij} \frac{\triangle_y u^n_{i,j}}{|\triangle_y u^n_{i,j}|_\epsilon} \right) + \triangle_{xy} \left(\alpha_{ij} \frac{\triangle_{xy} u^n_{i,j}}{|\triangle_{xy} u^n_{i,j}|_\epsilon} \right) \right], \\ \alpha_{i,j} &= \frac{1}{\sqrt{1 + |G_\sigma * \nabla u_0(x)|^2_{i,j}}}, \quad |\cdot|_\epsilon = |\cdot| + \epsilon, \quad \epsilon > 0, \\ u^0_{i,j} &= u_0(ih, jh), \qquad 0 \le i \le I, 0 \le j \le J, \\ u^n_{i,0} &= u^n_{i,1}, \quad u^n_{0,j} = u^n_{1,j}, \qquad u^n_{I,j} = u^n_{I-1,j}, \qquad u^n_{i,J} = u^n_{i,J-1}, \\ u^n_{i,0} &= 0, \quad u^n_{0,j} = 0, \quad u^n_{I,j} = 0, \quad u^n_{i,J} = 0. \end{aligned}$$

Here the MATLAB function "conv2" is used to represent the two-dimensional discrete Convolution Transform of the matrix $u_{i,j}$.

5. Numerical experiments

In this section, we demonstrate the performance of our model in denoising images involving Gaussian white noise. We applied difference equations discussed in section 4 and compared the

results with the results of ROF model [18] and PM model [17]. We used step size $\tau = 0.02$, gride size $h = 1$ and $\lambda = 0$.

At the end of the denoising process, the peak signal to noise ratio (PSNR), mean absolute-deviation error (MAE) and structure similarity index measure (SSIM) values were recorded to measure the denoising performance. The values are given by the following formulas:

$$\mathrm{PSNR}(u, u_0) = 10 \log_{10} \frac{IJ|\max u_0 - \min u_0|^2}{\|u - u_0\|_{L^2}^2} \mathrm{dB}$$

and

$$\mathrm{MAE}(u, u_0) = \frac{\|u - u_0\|_{L^1}}{IJ},$$

where $|\max u_0 - \min u_0|$ gives the gray-scale range of the original image, u_0 and u denote, respectively, the original image and the denoised image, $I \times J$ is the dimension of image.

SSIM, designed by Wang et al. [21], is a quality used to measure the similarity between any two images. Given any two images u and u_0, SSIM is given by the formula

$$\mathrm{SSIM}(u, u_0) = \mathrm{L}(u, u_0) \cdot \mathrm{C}(u, u_0) \cdot \mathrm{R}(u, u_0).$$

$\mathrm{L}(u, u_0) = \frac{2\mu_u\mu_{u_0}+k_1}{\mu_u^2+\mu_{u_0}^2+k_1}$, compares the two images' mean luminance μ_u and μ_{u_0}. The maximal value of $\mathrm{L}(u, u_0) = 1$, if $\mu_u = \mu_{u_0}$, $\mathrm{C}(u, u_0) = \frac{2\sigma_u\sigma_{u_0}+k_2}{\sigma_u^2+\sigma_{u_0}^2+k_2}$, measures the closeness of contrast of the two images u and u_0. Contrast is determined in terms of standard deviation, σ. Contrast comparison measure $\mathrm{C}(u, u_0) = 1$ maximally if and only if $\sigma_u = \sigma_{u_0}$; that is, when the images have equal contrast.

$\mathrm{R}(u, u_0) = \frac{\sigma_{uu_0}+k_3}{\sigma_u\sigma_{u_0}+k_3}$, is a structure comparison measure which determines the correlation between the images u and u_0, where σ_{uu_0} is covariance between u and u_0. It attains maximal value of 1 if, structurally, the two images coincide, but its value is equal to zero when there is absolutely no structural coincidence. The quantities k_1, k_2 and k_3 are small positive perturbations that avert the possibility of having zero denominators.

Two test images of "Cameraman" and "Peppers" are corrupted by white Gaussian noise with standard deviation (SD) of 30, (Figures 1 and 2). Tables 1 and 2, present the numerical results of restoration of Cameraman image, (Figure 1), and those of the Peppers image, (Figure 2). The comparisons are based on PSNR, MAE and SSIM. The proposed method shows the best performance with respect to PSNR, MAE and SSIM.

Our first example is Cameraman image, which is displayed in Figure 1(a) and 1(b) is its degraded version. Furthermore, Figure 1(c), 1(d) and 1(e), are portions of the recovered images with the proposed model, ROF model and PM model, respectively. It is clear that our method can overcome the staircase effect that caused by the second order method.

The second example is Peppers image, which is displayed in Figure 2(a), its degraded version is showed in Figure 2(b). Basically, Figure 2(c), 2(d) and 2(e), are portions of the recovered images by the proposed model, ROF model and PM model, respectively. It is evident that, our method yields good results in restoring image since it avoids the staircase effect that caused by the second order method while, at the same time, handle edges in a best way.

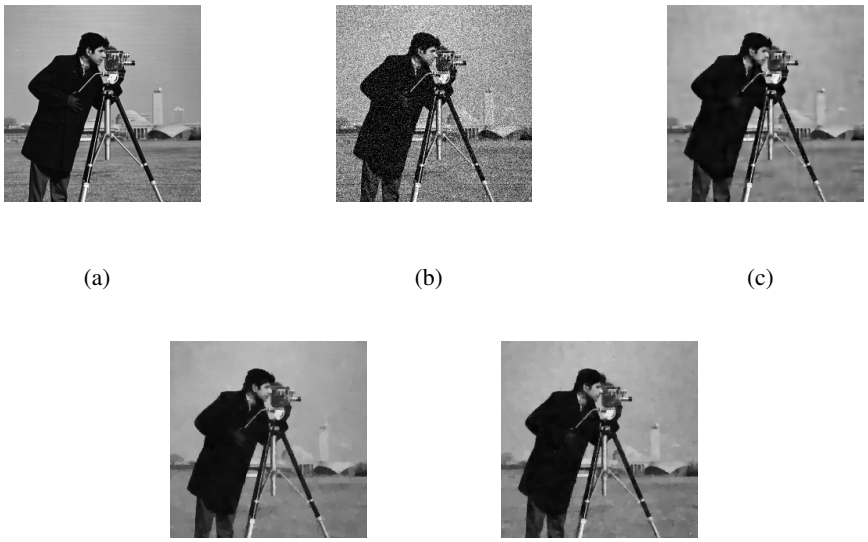

(a) (b) (c)

(d) (e)

Figure 1. Cameraman image, a portion of the results achieved with different models, (251×251). (a) Original image. (b) Noisy image corrupted by Gaussian noise for $\sigma = 30$. (c) Our method. (d) ROF model. (e) PM model.

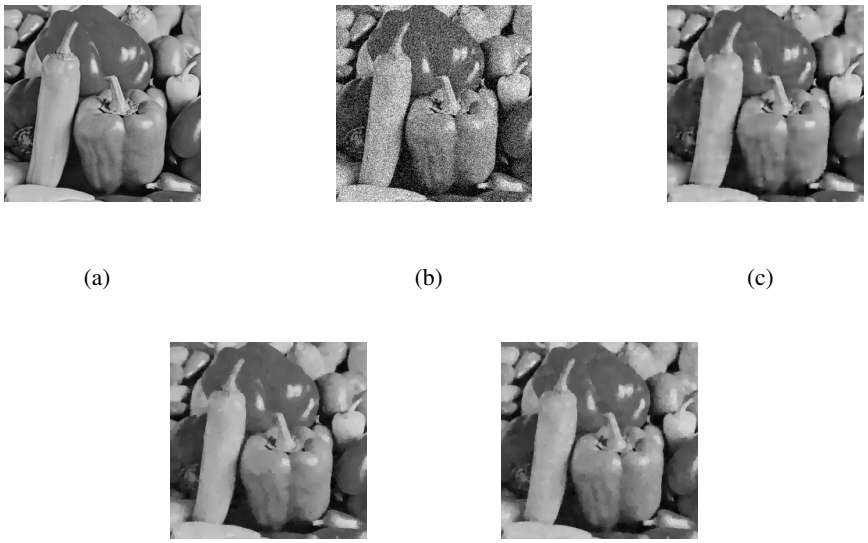

(a) (b) (c)

(d) (e)

Figure 2. Peppers image, a portion of the results achieved with different models, (251×251). (a) Original image. (b) Noisy image corrupted by Gaussian noise for $\sigma = 30$. (c) Our method. (d) ROF model. (e) PM model.

Table 1. Numerical results for Peppers image (251×251) experiment, Figure 2.

Algorithm	σ	PSNR	MAE	SSIM
PM model	30	27.98	7.06	0.8345
ROF model	30	28.26	6.80	0.8359
Our Method	30	**28.66**	**6.44**	**0.8537**

Table 2. Numerical results for Cameraman image (251×251) experiment, Figure 3.

Algorithm	σ	PSNR	MAE	SSIM
PM model	20	28.89	5.83	0.8386
ROF model	20	28.76	5.85	0.8397
Our Method	20	**29.04**	**5.62**	**0.8450**

Similarly, the two test images are corrupted by white Gaussian noise with SD of 20, (Figures 3 and 4). Tables 3 and 4, present the numerical results of restoration of Cameraman image, (Figure 3), and those of the Peppers image, (Figure 4). The comparisons are based on PSNR, MAE and SSIM. Here again, the proposed method shows the best performance with respect to PSNR, MAE and SSIM. In Figure 3(a) and 3(b) we display Cameraman image and the noisy version. Figure 3(c), 3(d) and 3(e), are portions of the recovered images with the proposed model, ROF model and PM model, respectively. We display Peppers image and the degraded version in Figure 4(a) and 4(b). Figure 4(c), 4(d) and 4(e), are portions of the recovered images with the proposed model, ROF model and PM model, respectively. Here also, the proposed model yields better results in denoising image while handling edges in a best way.

Table 3. Numerical results for Peppers image (251×251) experiment, Figure 4.

Algorithm	σ	PSNR	MAE	SSIM
PM model	20	29.86	5.70	0.8727
ROF model	20	29.90	5.64	0.8741
Our Method	20	**30.48**	**5.18**	**0.8795**

Table 4. Numerical results of Barbara and Lena images.

Image	Algorithm	σ	PSNR	MAE	SSIM
Lena	YK	30	26.08	8.62	0.7275
	LLT	30	27.10	8.11	0.7554
	Ours	30	**27.46**	**7.11**	**0.8078**
	YK	20	27.73	6.97	0.8082
	LLT	20	29.18	6.39	0.8211
	Ours	20	**29.20**	**5.89**	**0.8421**
Barbara	YK	30	25.80	9.31	0.7053
	LLT	30	26.83	8.69	0.7258
	Ours	30	**27.07**	**8.00**	**0.7520**
	YK	20	27.13	7.98	0.7584
	LLT	20	28.28	7.29	0.7794
	Ours	20	**28.46**	**6.79**	**0.7945**

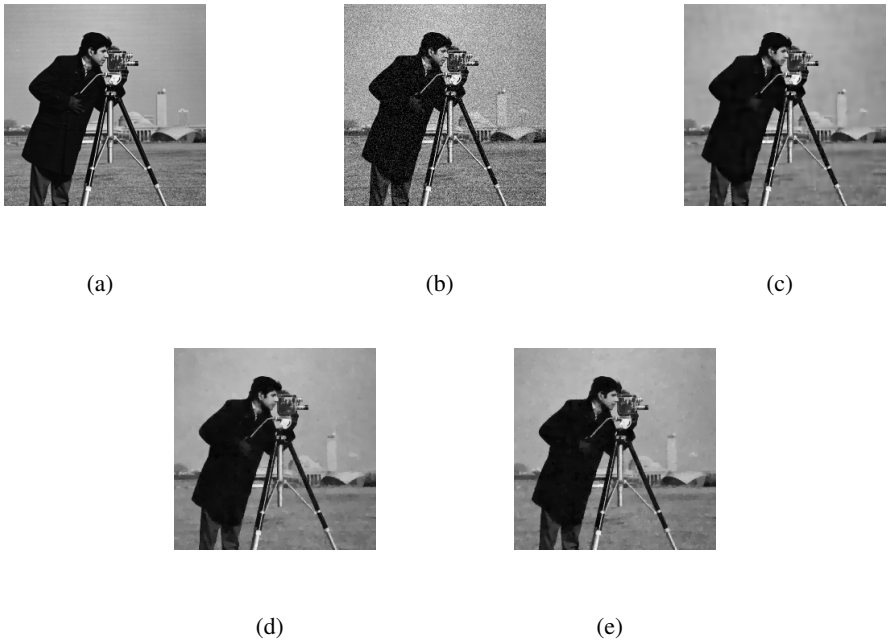

(a) (b) (c)

(d) (e)

Figure 3. Cameraman image, a portion of the results achieved with different models, (251×251). (*a*) Original image. (*b*) Noisy image corrupted by Gaussian noise for $\sigma = 20$. (*c*) Our method. (*d*) ROF model. (*e*) PM model.

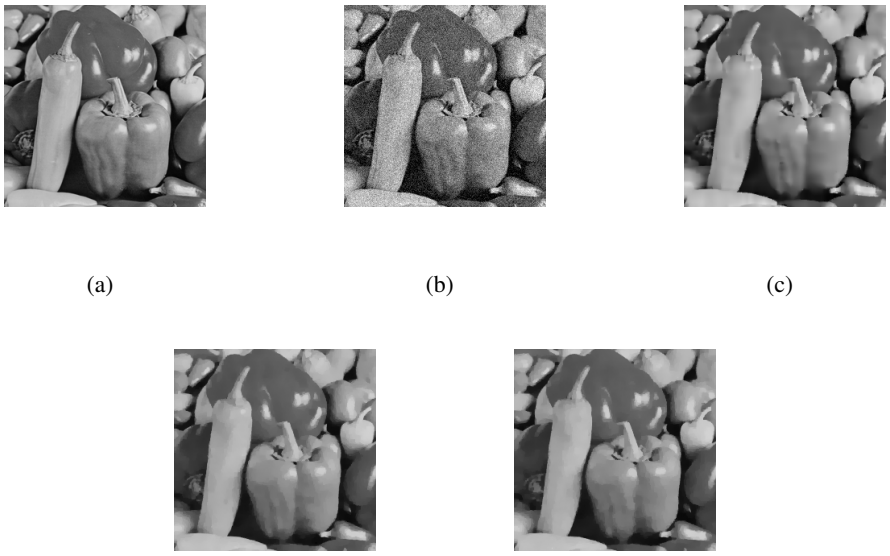

(a) (b) (c)

(d) (e)

Figure 4. Peppers image, a portion of the results achieved with different models, (251×251). (*a*) Original image. (*b*) Noisy image corrupted by Gaussian noise for $\sigma = 20$. (*c*) Our method. (*d*) ROF model. (*e*) PM model.

Not surprisingly, although the edges are preserved, the staircase effect is visible for the second order models, and there are some speckles in the processed images, with an example given in Figure 2. Comparing the images processed by our model and the original images, we can observed that, the differences are insignificant. The edges are preserved and no speckles appear in the processed images.

Finally, to illustrate the superiority of the proposed model over other related fourth-order models, we compared our results with YK model [26] and LLT model [16]. Barbara and Lena images have been corrupted by white Gaussian noise with SD of 30 (Figures 5 and 6) and SD of 20 (Figures 7 and 8). Numerical results for the images are tabulated in Table 4. Besides getting better outcomes, as evident from the results (see Figures 5 and 6), the model tackles the speckles caused by YK model at the same time.

In Figures 6 and 8, the results of Lena Image have been displayed. In Figure 6, the test image Lena and its noisy version degraded by Gaussian noise with SD of 30 are shown in the sections (a) and (b), sections (c) to (e) are the results of the YK model, LLT model and the proposed one. Similarly, in Figure 8, the test image Lena and its noisy version degraded by Gaussian noise with SD of 20 are shown with the same order described above. The last image in section (e) of Figures 6 and 8 are the results of our suggested filter in which the extent of the denoising performance is noticeably better than competitor filter.

(a) (b) (c)

(d) (e)

Figure 5. Barbara image, a portion of the results achieved with different models, (251×251). (*a*) Original image. (*b*) Noisy image corrupted by Gaussian noise for $\sigma = 30$. (*c*) YK model. (*d*) LLT model. (*e*) Our method.

(a) (b) (c)

(d) (e)

Figure 6. Lena image, a portion of the results achieved with different models, (251 × 251). (*a*) Original image. (*b*) Noisy image corrupted by Gaussian noise for $\sigma = 30$. (*c*) YK model. (*d*) LLT model. (*e*) Our method.

(a) (b) (c)

(d) (e)

Figure 7. Barbara image, a portion of the results achieved with different models, (251×251). (*a*) Original image. (*b*) Noisy image corrupted by Gaussian noise for $\sigma = 20$. (*c*) YK model. (*d*) LLT model. (*e*) Our method.

(a) (b) (c)

(d) (e)

Figure 8. Lena image, a portion of the results achieved with different models, (251 × 251). (*a*) Original image. (*b*) Noisy image corrupted by Gaussian noise for $\sigma = 20$. (*c*) YK model. (*d*) LLT model. (*e*) Our method.

6. Conclusions

In this article, we proposed a fourth-order image denoising model. The model was based on solving a fourth order partial differential equation by defining its corresponding functional. We proved, by use of Rothe's method, the existence and uniqueness of the entropy solution of the equation. Compared with the well known ROF and PM models, numerical results showed that our model perform better image recovery and can overcome staircase effects.

Conflict of interest

The authors declare that they have no conflict of interests whatsoever and do approve the publication of this paper.

References

1. T. Barbu, PDE-based restoration model using nonlinear second and fourth order diffusions, *Proc. Romanian Acad. Ser. A,* **16** (2015), 138–146.
2. T. Barbu, I. Munteanu, A nonlinear fourth-order diffusion-based model for image denoising and restoration, *Proc. Romanian Acad. Ser. A,* **18** (2017), 108–115.
3. C. Brito-Loeza, K. Chen, V. Uc-Cetina, Image denoising using the gaussian curvature of the image surface, *Numer. Meth. Part. Differ. Equ.,* **32** (2016), 1066–1089.
4. L. Deng, H. Zhu, Z. Yang, Y. Li, Hessian matrix-based fourth-order anisotropic diffusion filter for image denoising, *Opt. Laser Technol.,* **110** (2019), 184–190.
5. I. Fonseca, G. Leoni, J. Malỳ, R. Paroni, A note on meyers' theorem in $W^{k,1}$, *Trans. Am. Math. Soc.,* **354** (2002), 3723–3741.
6. P. Guidotti, K. Longo, Well-posedness for a class of fourth order diffusions for image processing, *Nonlinear Differ. Equ. Appl. NoDEA,* **18** (2011), 407–425.
7. Z. Guo, J. Yin, Q. Liu, On a reaction-diffusion system applied to image decomposition and restoration, *Math. Comput. Modell.,* **53** (2011), 1336–1350.
8. W. Hinterberger, O. Scherzer, Variational methods on the space of functions of bounded hessian for convexification and denoising, *Computing,* **76** (2006), 109–133.
9. A. Laghrib, A. Chakib, A. Hadri, A. Hakim, A nonlinear fourth-order pde for multi-frame image super-resolution enhancement, *Discrete Cont. Dyn. Syst.-B,* **25** (2020), 415.
10. A. Laghrib, A. Hadri, A. Hakim, An edge preserving high-order pde for multiframe image super-resolution, *J. Franklin Inst.,* **356** (2019), 5834–5857.
11. F. Li, C. Shen, J. Fan, C. Shen, Image restoration combining a total variational filter and a fourth-order filter, *J. Vis. Commun. Image R.,* **18** (2007), 322–330.
12. G. Liu, T. Z. Huang, J. Liu, High-order TVL1-based images restoration and spatially adapted regularization parameter selection, *Comput. Math. Appl.,* **67** (2014), 2015–2026.
13. Q. Liu, Z. Yao, Y. Ke, Entropy solutions for a fourth-order nonlinear degenerate problem for noise removal, *Nonlinear Anal.,* **67** (2007), 1908–1918.

14. X. Liu, L. Huang, Z. Guo, Adaptive fourth-order partial differential equation filter for image denoising, *Appl. Math. Lett.,* **24** (2011), 1282–1288.

15. X. Liu, C. H. Lai, K. Pericleous, A fourth-order partial differential equation denoising model with an adaptive relaxation method, *Int. J. Comput. Math.,* **92** (2015), 608–622.

16. M. Lysaker, A. Lundervold, X. C. Tai, Noise removal using fourth-order partial differential equation with applications to medical magnetic resonance images in space and time, *IEEE Trans. Image Proc.,* **12** (2003), 1579–1590.

17. P. Perona, J. Malik, Scale-space and edge detection using anisotropic diffusion, *IEEE Trans. Pattern Anal. Mach. Intell.,* **12** (1990), 629–639.

18. L. I. Rudin, S. Osher, E. Fatemi, Nonlinear total variation based noise removal algorithms, *Phys. D: Nonlinear Phenom.,* **60** (1992), 259–268.

19. D. M. Strong, *Adaptive total variation minimizing image restoration*, Department of Mathematics, University of California, Los Angeles, 1997.

20. L. Sun, K. Chen, A new iterative algorithm for mean curvature-based variational image denoising, *BIT Numer. Math.,* **54** (2014), 523–553.

21. Z. Wang, A. C. Bovik, H. R. Sheikh, E. P. Simoncelli, Image quality assessment: From error visibility to structural similarity, *IEEE Trans. Image Proc.,* **13** (2004), 600–612.

22. Y. Wen, J. Sun, Z. Guo, A new anisotropic fourth-order diffusion equation model based on image feature for image denoising, *CAM report,* 2020.

23. Z. Wu, J. Yin, C. Wang, *Elliptic & parabolic equations*, World Scientific Publishing Company Incorporated, 2006.

24. X. Y. Liu, C. H. Lai, K. A. Pericleous, A fourth-order partial differential equation denoiding model with an adaptive relaxation method, *Int. J. Comut. Math.,* **92** (2015), 608–622.

25. Q. Yang, Image denoising combining the P-M model and the LLT model, *J. Comput. Commun.,* **3** (2015), 22–30.

26. Y. L. You, M. Kaveh, Fourth-order partial differential equations for noise removal, *IEEE Trans. Image Proc.,* **9** (2000), 1723–1730.

27. X. Zhang, W. Ye, An adaptive fourth-order partial differential equation for image denoising, *Comput. Math. Appl.,* **74** (2017), 2529–2545.

28. W. Zhu, T. Chan, Image denoising using mean curvature of image surface, *SIAM J. Imaging Sci.,* **5** (2012), 1–32.

AIMS Press